

Three-dimensional Bose-Fermi droplets at nonzero temperatures

Maciej Lewkowicz,¹ Mirosław Brewczyk,² Mariusz Gajda,³ and Tomasz Karpiuk²

¹ *Doctoral School of Exact and Natural Sciences, University of Białystok, ul. K. Ciołkowskiego 1K, 15-245 Białystok, Poland*

² *Wydział Fizyki, Uniwersytet w Białymstoku, ul. K. Ciołkowskiego 1L, 15-245 Białystok, Poland*

³ *Institute of Physics, Polish Academy of Sciences, Aleja Lotników 32/46, PL-02668 Warsaw, Poland*

(Dated: February 24, 2026)

Using numerical methods, we study the formation of self-bound quantum Bose-Fermi droplets at nonzero temperatures. We describe an attractive atomic Bose-Fermi mixture using quantum hydrodynamics enriched by beyond-mean-field corrections and thermal fluctuations, together with a simplified self-consistent Hartree-Fock model. With these models, we determine that low-temperature droplets with finite lifetimes can exist in free space when the attraction between bosons and fermions is sufficiently strong. Additionally, Bose-Fermi droplets at nonzero temperatures can exist in a box potential in equilibrium with bosonic and fermionic vapor. We discuss the properties of Bose-Fermi droplets at nonzero temperatures in terms of the initial condensate fraction, total atom number, and interspecies attraction strength.

I. INTRODUCTION

Since the first experimental achievement of quantum degeneracy in fermionic potassium and lithium gases [1–5], interest in ultracold mixtures with a fermionic component has grown rapidly. Studies of many-body quantum phenomena, including equilibrium and nonequilibrium thermodynamic properties [6–8], correlations [9–11], strong interactions in lower dimensions [12, 13], and dipolar effects [14–16], soon followed.

A novel quantum mixture – a self-bound system of ultracold atoms – has been realized experimentally in recent years. The first quantum droplets were observed in a gas of dysprosium-164 atoms [17]. The interplay of short-range and dipolar forces turned out to be crucial for stabilizing such systems. Other dipolar droplets were created using erbium-166 atoms [18]. The existence of a different kind of self-bound object – droplets in a two-component mixture of bosonic potassium-39 atoms – was soon demonstrated [19, 20]. Quantum droplets in heteronuclear bosonic mixtures were also observed [21].

Another class of self-bound system – Bose-Fermi droplets – has recently been introduced at the theoretical level [22, 23]. Such systems may bring a variety of physical phenomena into play, including connections to polaron physics, Cooper pairing, and fermionic superfluidity. Analogies can also be drawn with astronomical objects such as white dwarfs, due to the stabilization mechanism involving Fermi pressure. The quantum aspects of the disruption of a white dwarf star by a black hole have recently been modeled [24, 25], in connection with observations of recurrent ultraluminous X-ray flares [26, 27].

The aim of this paper is to answer the question of whether three-dimensional Bose-Fermi droplets exist at nonzero temperatures. Similar studies related to attractive binary Bose droplets have already been reported using the exact path-integral Monte Carlo method (see Refs. [28] and [29]). Using the hydrodynamic description, we find that Bose-Fermi droplets in free space exist

at finite temperatures. They cool down to zero temperature within a finite amount of time by emitting bosonic and fermionic atoms. In a box potential, Bose-Fermi droplets cool down to a nonzero temperature via a similar mechanism and coexist with bosonic and fermionic vapors. This last finding is confirmed by a simplified, equilibrium-based approach.

The paper is organized as follows. In Sec. II, we propose a method for studying the formation of nonzero temperature Bose-Fermi droplets. Specifically, we develop a numerical technique to measure the droplet's temperature. Then, in Sec. III, we discuss the evolution and properties of a nonzero temperature Bose-Fermi droplets. We consider two cases: when the droplet is in free space and when it is confined in a box (i.e., immersed in bosonic and fermionic vapors). In the first scenario, the droplet's lifetime is limited, and it cools down to zero temperature. Depending on the number of atoms and/or the strength of interparticle attraction, the Bose-Fermi droplet either survives or melts. We conclude in Sec. III.

II. THERMOMETRY

To study Bose-Fermi droplets at nonzero temperatures, we apply the following procedure. First, we determine the bosonic and fermionic densities for a mixture confined in a spherically symmetric trap at zero temperature, for a given boson-fermion attraction strength. To do so, we solve the set of hydrodynamic equations (A1) and (A2) using the imaginary-time technique [30, 31]. Next, we slowly pump energy into the mixture by randomizing the amplitude and phase of the zero-temperature bosonic field at each point of a numerical grid and evolving Eqs. (A1) and (A2) in real time. The strength of the randomization determines the amount of energy injected into the system. Since both components are coupled, the injected energy spreads throughout the binary mixture. Assuming the energy is injected sufficiently slowly, the final state remains close to equilibrium,

which can be verified by the characteristic dynamics of the condensate fraction that, in the final stages, does not change but only fluctuates around a mean value. Thus, a Bose-Fermi mixture in a state close to equilibrium is obtained. The condensate fraction is then below 1, although the exact temperature of the sample – clearly nonzero – remains unknown. Finally, we open the trap and observe the subsequent dynamics of the Bose-Fermi mixture. This part of the procedure could, in principle, be realized experimentally. Non-spreading bosonic and fermionic densities indicate the formation of a self-bound Bose-Fermi droplet. Depending on the boundary conditions, we can observe either the evolution of a droplet at nonzero temperature in free space or the equilibrium dynamics of a droplet immersed in a saturated vapor of bosonic and fermionic atoms.

An example illustrating the outcome of the above prescription is shown in Fig. 1, where the condensate, thermal, total, and fermionic column densities (i.e., densities integrated along one spatial dimension) are plotted in blue, red, black, and green solid lines, respectively. These curves are obtained within the hydrodynamic description for the interspecies scattering length $a_{BF}/a_B = -3$ and trapping frequencies of $2\pi \times 250$ Hz for bosons and $2\pi \times 4000$ Hz for fermions. We consider mixtures composed of ^{133}Cs bosonic and ^6Li fermionic atoms, which are currently studied experimentally [32–35]. The numbers of bosons and fermions are specified in the figure caption.

After equilibration, we adopt a technique commonly used within the classical fields approximation to describe bosonic systems at nonzero temperatures [36]. This standard procedure allows us to determine the condensate fraction, which is found to be $n_0 = 0.4$. We then apply thermometry based on the self-consistent Hartree-Fock method, as described in Appendix B. The corresponding densities are shown as dashed lines in Fig. 1. They are obtained by matching the temperature so as to reproduce the same condensate fraction, $n_0 = 0.4$, which yields $T = 286$ nK.

A summary of the thermometry procedure is presented in Fig. 2 for four sets of boson and fermion numbers, as indicated in the legend, with $a_{BF}/a_B = -3$ (top panel), and for four samples distinguished by their mutual scattering lengths (given in the legend) with $N_B = 1460$ and $N_F = 100$ (bottom panel).

III. BOSE-FERMI DROPLETS AT NONZERO TEMPERATURES

We now investigate the formation and properties of Bose-Fermi droplets at nonzero temperatures. The bosonic and fermionic densities presented in Fig. 1 are used as the initial conditions for the subsequent real-time evolution. Starting from these densities, we rapidly remove the trapping potential (within about 3.6 ms, approximately one oscillation period of the bosonic trap)

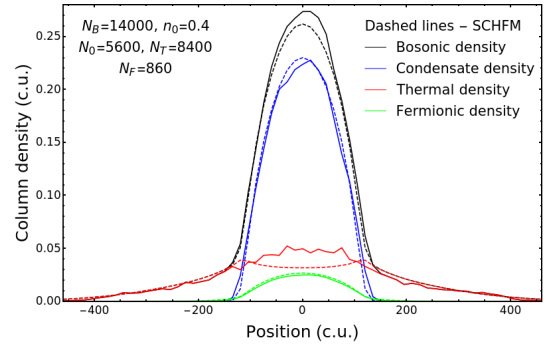


FIG. 1: Column densities of a condensate and thermal fraction and of fermionic component for $a_{BF}/a_B = -3$ and the trapping frequencies $2\pi \times 250$ Hz and $2\pi \times 4000$ Hz for bosons and fermions, respectively. The number of condensate, thermal, and fermionic atoms is $N_0 = 5600$, $N_{th} = 8400$, and $N_F = 860$. The temperature of the sample is $T = 286$ nK which corresponds to the condensate fraction $n_0 = 0.4$. Solid lines show the results obtained using the hydrodynamic approach while the dashed lines comes from the simplified self-consistent Hartree-Fock treatment.

and monitor the evolution of the mixture. We consider two scenarios determined by the applied boundary conditions. Absorbing boundary conditions correspond to a droplet (or Bose-Fermi mixture) evolving in free space, whereas periodic boundary conditions mimic confinement in a box potential. In the following, we analyze the properties of Bose-Fermi droplets with respect to the initial condensate fraction (i.e., temperature), the total atom number, and the strength of the interspecies attraction.

A. Droplet evolution as a function of condensate fraction

Fig. 3 illustrates the bosonic column densities obtained using the hydrodynamic prescription for different amounts of energy injected into the system. The sample remains trapped, and the resulting equilibrium states correspond to a wide range of condensate fractions, from very small to large. The mixture contains $N_B = 14000$ bosons and $N_F = 860$ fermions, and the thermal fraction increases from top to bottom. The bosons and fermions interact attractively with $a_{BF}/a_B = -3$.

Then, the trap is opened. Fig. 4 shows the condensate fraction (upper panel) and the bosonic and fermionic norms (lower panel) at later times. When the initial condensate fraction is set to 0.4, the corresponding density is given by the red curve in Fig. 3. Clearly, the droplet cools under both absorbing (solid lines) and periodic (dotted lines) boundary conditions, as evidenced by the increase of the condensate fraction over time.

In the case of absorbing boundary conditions (i.e., a droplet evolving in free space), the condensate fraction approaches unity, indicating that the droplet temperature becomes very low, eventually approaching zero. Ex-

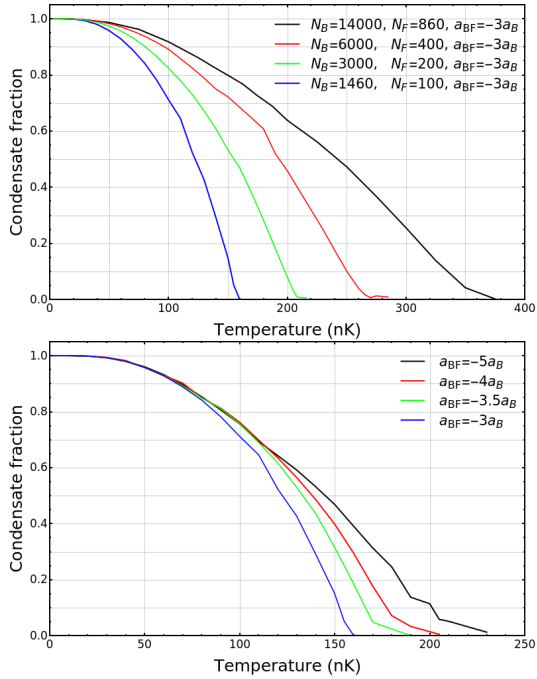


FIG. 2: Condensate fraction as a function of temperature. The top panel shows four samples distinguished by the number of atoms (given in the legend) and for $a_{BF}/a_B = -3$. The bottom panel shows four samples distinguished by the mutual scattering length (given in the legend) and for $N_B = 1460$ and $N_F = 100$. These curves were obtained by solving the self-consistent Hartree-Fock equations as described in Appendix B.

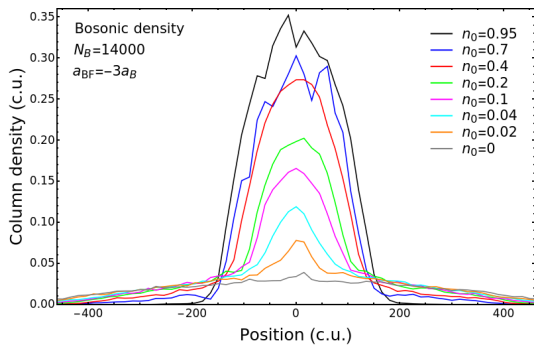


FIG. 3: Column densities for the bosonic component are shown for $a_{BF}/a_B = -3$ and for different amounts of energy pumped into the system. The number of bosonic atoms is $N_B = 14000$, and the condensate fraction is indicated in the legend. These results were obtained using the hydrodynamic approach.

cess bosonic and fermionic atoms are removed through the boundaries, leading to a gradual decrease of their norms (see the lower panel of Fig. 4). For periodic boundary conditions, corresponding to a droplet in a finite volume, the system also cools by expelling atoms into the surrounding vapor. This process eventually saturates, and the condensate fraction reaches a steady value be-

low unity. The final state is a Bose-Fermi droplet in equilibrium with bosonic and fermionic vapor. The total number of particles is conserved thus the norms of both components remain equal to one.

The movies available at Refs. [37] and [38] show the evolution of the bosonic and fermionic column densities after the trap is opened. For a droplet evolving in free space [37], a form of self-evaporative cooling takes place. The most energetic atoms are no longer confined once the trap is removed and escape from the mixture, while the remaining atoms equilibrate at a lower temperature. This process continues until the bosonic component becomes an almost pure condensate. The initial stages of the evolution are rather violent due to large fluctuations in the thermal component; however, at later times the droplet becomes quiet, with a nearly stationary surface.

In contrast, when the droplet is confined to a finite volume [38], its dynamics remain violent even after equilibrium with the surrounding vapor is established. The droplet is continuously hit by thermal atoms and exhibits irregular motion resembling a form of Brownian motion.

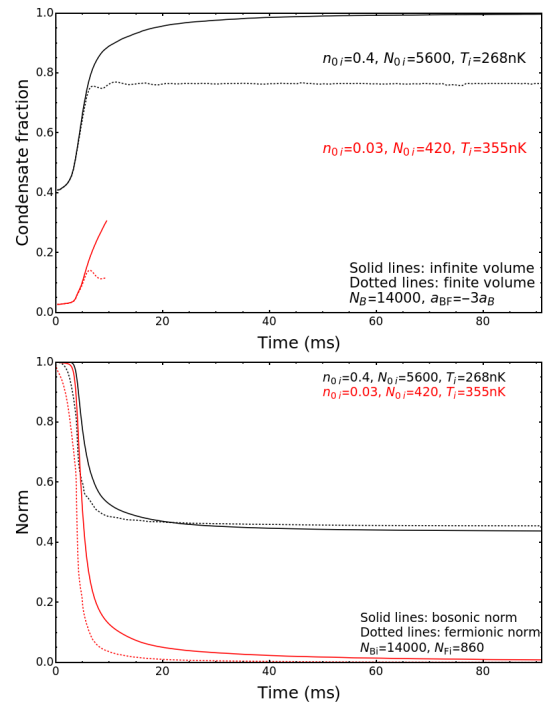


FIG. 4: (a) Condensate fraction as a function of time for the absorbing (solid line) and periodic (dotted line) boundary conditions. (b) Number of bosons (solid line) and fermions (dotted line) as a function of time for absorbing boundary conditions. The initial number of atoms is $N_B = 14000$ and $N_F = 860$, and $a_{BF}/a_B = -3$. The temperatures are 268 nK (black lines) and 355 nK (red lines), which corresponds to condensate fractions of 0.4 and 0.03, respectively.

The fate of a Bose-Fermi droplet depends on the initial condensate fraction. For a sufficiently small initial condensate fraction ($n_0 < 0.04$, with other parameters as in Fig. 4), the number of atoms in the droplet falls be-

low the critical value required for its stability as it cools. Consequently, the droplet rapidly expels all atoms and disappears. The red lines in Fig. 4 show the condensate fraction (upper panel) and the norm (lower panel) for an initial condensate fraction of 0.03. Both norms clearly drop to zero very quickly.

As in the previous case, the condensate fraction initially grows as the droplet cools by ejecting the most energetic atoms. Monitoring the condensate fraction for times longer than 10 ms is not meaningful because the size of the condensate cloud exceeds the numerical grid used for its calculation. The movie available at Ref. [39] illustrates the droplet's explosion occurring after approximately 6 ms.

B. Droplet evolution as a function of the total number of atoms and interspecies attraction

We now study the evolution of thermal Bose-Fermi droplets as a function of the initial total number of atoms. In the phase diagram shown in Fig. 5, the region above the black curve corresponds to conditions under which stationary droplets are eventually formed, assuming $a_{BF}/a_B = -3$ (as in Fig. 4). Points on the curve indicate the critical initial condensate fraction required for droplet formation after releasing the atoms from the trap into free space. Clearly, the fate of the system depends on both the initial number of atoms and the condensate fraction, which directly relates to the amount of thermal energy, i.e., the temperature.

For a boson number of $N_B = 1460$ (the leftmost point in Fig. 5), the critical initial condensate fraction is larger than in the case studied in the previous subsection (corresponding to the rightmost point in Fig. 5). As expected, for smaller atom numbers, thermal energy more easily drives evaporation and atom loss; hence, stable droplets are obtained only for larger initial condensate fractions. Although the phase diagram in Fig. 5 was obtained using absorbing boundary conditions, similar conclusions hold when using periodic boundary conditions.

Further understanding of droplet evaporation can be gained by examining Fig. 6, which shows the phase diagram plotted in terms of the strength of the components' mutual attraction and the initial condensate fraction. The minimal numbers of bosons and fermions, N_{Bc} and N_{Fc} , respectively, required to support a stable free droplet at zero temperature are indicated in the figure.

When a droplet initially at nonzero temperature is released from the trap, it expels atoms on its way toward an equilibrium. These expelled atoms are removed from the system through absorbing boundary conditions, leading to a gradual decrease in the total number of bosons and fermions. At some point, the number of bosons may drop below the black line in Fig. 6, causing the droplet to disappear by rapidly ejecting the remaining atoms. Note that the black line closely matches the zero-temperature droplet data in free space in terms of the number of

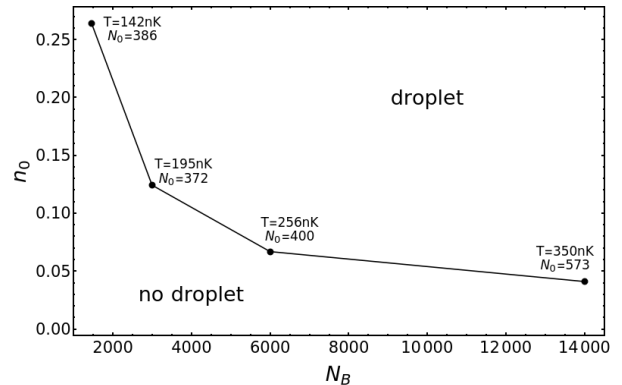


FIG. 5: Phase diagram showing the region in which Bose-Fermi droplets exist, as a function of total number of bosons and the initial (i.e., before opening the trap) condensate fraction, for $a_{BF}/a_B = -3$. The number of fermions is $N_F = N_B/14.6$. Too high temperature (too low condensate fraction) destroys the droplet after the trap is removed. The data (T, N_0) displayed in the diagram show the highest temperature at which the droplet is not destroyed and the corresponding number of condensed atoms for an initial total number of bosonic atoms N_B , as shown on the x -axis.

bosonic and fermionic atoms. For $a_{BF}/a_B = -3$ and an initial number of bosons $N_B = 1460$, a droplet with as few as 400 condensed bosons remains stable (see also Fig. 5). Initial temperature of this droplet equals approximately 140 nK.

To stabilize even smaller droplets, the attraction between bosons and fermions must be stronger (see Fig. 6). For example, with $a_{BF}/a_B = -5$, a Bose-Fermi droplet with an initial $N_B = 50$ bosons (at a temperature of approximately 220 nK) can survive the opening of the trap (corresponding to the far-left point in Fig. 6). However, such small droplets are highly sensitive to disturbances from thermal atoms during cooling and can be even shifted to random positions; see the movie at Ref. [40].

IV. CONCLUSIONS

In summary, we have studied the formation of Bose-Fermi droplets at nonzero temperatures using a hydrodynamic description. These droplets exist when the boson-fermion attraction is sufficiently strong. We demonstrate that their lifetime is limited and that they cool by emitting bosonic and fermionic particles. In free space, they eventually reach zero temperature and thus act as nearly perfect coolers. When confined in a box, the droplets attain equilibrium with the surrounding saturated bosonic and fermionic vapors.

Whether a droplet survives or explodes in free space depends on the initial number of atoms and the temperature for a given boson-fermion attraction strength (see Fig. 5). Nonzero-temperature Bose-Fermi droplets could provide a model for the early-stage cooling of helium white dwarf stars via a hypothetical mechanism in-

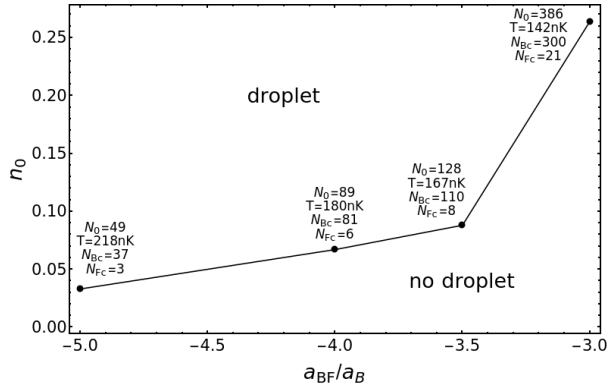


FIG. 6: Phase diagram showing the region in which Bose-Fermi droplets exist as a function of interspecies attraction and the initial condensate fraction (i.e., the fraction of atoms in the condensate before opening the trap), for an initial number of bosons of $N_B = 1460$. The displayed data (T, N_0) show the maximum temperature at which the droplet survives opening the trap and the corresponding number of condensed atoms. The additional data, (N_{Bc}, N_{Fc}), show the critical numbers of bosons and fermions, respectively, for a free droplet at zero temperature. This shows that the population of atomic droplets at the stability border decreases as boson-fermion attraction increases. A similar trend occurs with the ratio N_B/N_F . This is also true for infinitely large stable droplets (see Fig. 1 in Ref. [22]). A too-small number of atoms does not allow for the formation of a droplet, and when the temperature is nonzero, it destroys the droplet after the trap is removed.

volving the emission of energetic matter components.

Acknowledgments

M.B., M.G., and T.K. acknowledge support from the (Polish) National Science Center Grant No. 2017/25/B/ST2/01943. Part of the results were obtained using computers at the Computer Center of University of Bialystok.

Appendix A: Hydrodynamic equations

We rely on the hydrodynamic approach [41–48] to study the formation of atomic Bose-Fermi droplets at nonzero temperatures. In this approximation, the bosonic field, denoted by $\psi_B(\mathbf{r}, t)$, and the fermionic pseudo-field, denoted by $\psi_F(\mathbf{r}, t)$, are the fundamental variables. The bosonic field, also known as the classical field, encompasses all the bosonic atoms within the system, including those in a condensate and those in a thermal cloud (see Ref. [36]). The fermionic pseudo-field, specifically its square modulus and phase gradient, are interpreted as the density and velocity fields of a hydrodynamic fermionic fluid. The hydrodynamic equations of motion for the mixture are

$$i\hbar \frac{\partial}{\partial t} \psi_B = \left[-\frac{\hbar^2}{2m_B} \nabla^2 + \frac{1}{2} m_B \omega_B^2 r^2 + g_B n_B + g_{BF} n_F + \frac{5}{2} C_{LHY} n_B^{3/2} + C_{BF} n_F^{4/3} A(w, \alpha) + C_{BF} n_B n_F^{4/3} \frac{\partial A}{\partial \alpha} \frac{\partial \alpha}{\partial n_B} \right] \psi_B \quad (\text{A1})$$

and

$$i\hbar \frac{\partial}{\partial t} \psi_F = \left[-\frac{\hbar^2}{2m_F} \nabla^2 + (1 - \xi) \frac{\hbar^2}{2m_F} \frac{\nabla^2 |\psi_F|}{|\psi_F|} + \frac{1}{2} m_F \omega_F^2 r^2 + \frac{5}{3} \kappa_k n_F^{2/3} + g_{BF} n_B + \frac{4}{3} C_{BF} n_B n_F^{1/3} A(w, \alpha) + C_{BF} n_B n_F^{4/3} \frac{\partial A}{\partial \alpha} \frac{\partial \alpha}{\partial n_F} \right] \psi_F. \quad (\text{A2})$$

Note the presence of beyond mean-field corrections for boson-boson interactions (the term involving C_{LHY} factor in Eq. (A1)) and boson-fermion interactions (the last two terms in Eq. (A1) and Eq. (A2)). Here, $g_B = 4\pi\hbar^2 a_B/m_B$ and $g_{BF} = 2\pi\hbar^2 a_{BF}/\mu$ characterize the interactions between bosons and bosons and fermions, respectively, expressed via the s -wave scattering lengths a_B and a_{BF} . The bosonic, fermionic, and the reduced masses are m_B , m_F , and μ , respectively. Other coefficients are: $\kappa_k = (3/10) (6\pi^2)^{2/3} \hbar^2/m_F$, $C_{LHY} = 64/(15\sqrt{\pi}) g_B a_B^{3/2}$, $C_{BF} = (6\pi^2)^{2/3} \hbar^2 a_{BF}^2/2m_F$, and $\xi = 1/9$. The function $A(w, \alpha)$ has a form:

$$A(w, \alpha) = \frac{2(1+w)}{3w} \left(\frac{6}{\pi} \right)^{2/3} \int_0^\infty dk \int_{-1}^{+1} d\Omega \left[1 - \frac{3k^2(1+w)}{\sqrt{k^2 + \alpha}} \int_0^1 dq q^2 \frac{1 - \Theta(1 - \sqrt{q^2 + k^2 + 2kq\Omega})}{\sqrt{k^2 + \alpha + wk + 2q\omega\Omega}} \right], \quad (\text{A3})$$

where $w = m_B/m_F$ and $\alpha = 16\pi n_B a_B^3 / (6\pi^2 n_F a_B^3)^{2/3}$ are the dimensionless parameters and $\Theta()$ is the Heaviside step function. Spherically symmetric trapping is assumed with different frequencies for the bosonic and fermionic traps. The total densities of the bosons and fermions are calculated as $n_B = |\psi_B|^2$ and $n_F = |\psi_F|^2$, respectively. The set of Eqs. (A1) and (A2) was already used to observe the temperature effect on the breathing mode of a Bose-Einstein condensate immersed in a Fermi sea [46]. At very low temperatures, these equations enabled the study of the static and dynamic properties of self-bound quantum Bose-Fermi droplets [22, 47].

Appendix B: Self-consistent Hartree-Fock method

In this approximation, the equilibrium densities of bosons and fermions are self-consistently determined for

a given temperature based on semi-classical distribution functions. The semi-classical distribution functions for bosons and fermions are

$$f_{\mathbf{p}}^B(\mathbf{r}) = \frac{1}{e^{[\varepsilon_{\mathbf{p}}^B(\mathbf{r}) - \mu_B]/k_B T} - 1} \quad (\text{B1})$$

and

$$f_{\mathbf{p}}^F(\mathbf{r}) = \frac{1}{e^{[\varepsilon_{\mathbf{p}}^F(\mathbf{r}) - \mu_B]/k_B T} + 1}, \quad (\text{B2})$$

respectively. For bosons, the semi-classical single-particle excitation energies are given by

$$\begin{aligned} \varepsilon_{\mathbf{p}}^B(\mathbf{r}) &= \frac{\mathbf{p}^2}{2m_B} + 2g_B [n_0(\mathbf{r}) + n_{th}(\mathbf{r})] + V_{tr}^B(\mathbf{r}) \\ &+ \frac{\delta E_{LHY}}{\delta n_0} + \frac{\delta E_{BF}}{\delta n_0}, \end{aligned} \quad (\text{B3})$$

where $E_{LHY} = C_{LHY} \int d\mathbf{r} n_0^{5/2}(\mathbf{r})$ and $E_{BF} = C_{BF} \int d\mathbf{r} n_0(\mathbf{r}) n_F^{4/3}(\mathbf{r}) A(w, \alpha)$ and $n_0(\mathbf{r})$ and $n_{th}(\mathbf{r})$ are the condensate and thermal densities, respectively (see Ref. [49] for discussion of the semi-classical energies for nonzero temperature bosonic gas within the Hartree-Fock approximation). The thermal density for bosons is given as

$$n_{th}(\mathbf{r}) = \frac{1}{\lambda_B^3} g_{3/2} \{ e^{[\mu_B - V_{eff}^B(\mathbf{r})]/k_B T} \}, \quad (\text{B4})$$

where $\lambda_B = (2\pi\hbar^2/m_B k_B T)^{1/2}$ and

$$\begin{aligned} V_{eff}^B(\mathbf{r}) &= 2g_B [n_0(\mathbf{r}) + n_{th}(\mathbf{r})] + V_{tr}^B(\mathbf{r}) \\ &+ \frac{\delta E_{LHY}}{\delta n_0} + \frac{\delta E_{BF}}{\delta n_0}. \end{aligned} \quad (\text{B5})$$

Similarly, the single-particle excitation energies for fermions are

$$\varepsilon_{\mathbf{p}}^F(\mathbf{r}) = \frac{\mathbf{p}^2}{2m_F} + V_{tr}^F(\mathbf{r}) + \frac{\delta E_{BF}}{\delta n_F} \quad (\text{B6})$$

and the fermionic density becomes

$$n_F(\mathbf{r}) = \frac{1}{\lambda_F^3} f_{3/2} \{ e^{[\mu_F - V_{tr}^F(\mathbf{r}) - \delta E_{BF}/\delta n_F]/k_B T} \}, \quad (\text{B7})$$

where $g_{3/2}(\cdot)$ and $f_{3/2}(\cdot)$ functions are ones of the standard functions for bosons and fermions [50]. The chemical potential μ_B is determined from the formula (see Ref. [49])

$$\mu_B = g_B [n_0(\mathbf{r}) + 2n_{th}(\mathbf{r})] + V_{tr}^B(\mathbf{r}) + \frac{\delta E_{LHY}}{\delta n_0} + \frac{\delta E_{BF}}{\delta n_0}, \quad (\text{B8})$$

while μ_F is calculated from the normalization condition $N_F = \int d\mathbf{r} n_F(\mathbf{r})$.

Based on the above equations, we can iteratively find the condensate density, $n_0(\mathbf{r})$, the thermal density, $n_{th}(\mathbf{r})$, and the fermionic density, $n_F(\mathbf{r})$, for a given temperature and a specific number of bosonic and fermionic atoms. This is done in the following steps. First, given the normalized densities, $n_0(\mathbf{r})$, $n_{th}(\mathbf{r})$, and $n_F(\mathbf{r})$, the bosonic chemical potential is found from Eq. (B8) by choosing $\mathbf{r} = 0$. Next, the new thermal density ($n_{th}(\mathbf{r})$) is calculated based on Eq. (B4). Next, the new condensate density, $n_0(\mathbf{r})$, is obtained from Eq. (B8). Finally, a new fermionic density is determined from Eq. (B7) together with the value of the fermionic chemical potential by a normalization procedure. The whole cycle is then repeated until all densities converge. We slightly modify the above prescription: to find the condensate density, we solve the following differential equation (see Ref. [49])

$$\begin{aligned} i\hbar \frac{\partial}{\partial t} \psi_0(\mathbf{r}) &= \left\{ -\frac{\hbar^2}{2m_B} \nabla^2 + g_B [n_0(\mathbf{r}) + 2n_{th}(\mathbf{r})] \right. \\ &+ \left. V_{tr}^B(\mathbf{r}) + \frac{\delta E_{LHY}}{\delta n_0} + \frac{\delta E_{BF}}{\delta n_0} \right\} \psi_0(\mathbf{r}) \end{aligned} \quad (\text{B9})$$

and calculate the condensate density as $n_0(\mathbf{r}) = |\psi_0(\mathbf{r})|^2$.

-
- [1] B. DeMarco and D. S. Jin, *Science* **285**, 1703 (1999).
[2] A. G. Truscott, K. E. Strecker, W. I. McAlexander, G. B. Partridge, and R. G. Hulet, *Science* **291**, 2570 (2001).
[3] F. Schreck, L. Khaykovich, K. L. Corwin, G. Ferrari, T. Bourdel, J. Cubizolles, and C. Salomon, *Phys. Rev. Lett.* **87**, 080403 (2001).
[4] S. R. Granade, M. E. Gehm, K. M. O'Hara, and J. E. Thomas, *Phys. Rev. Lett.* **88**, 120405 (2002).
[5] Z. Hadzibabic, S. Gupta, C. A. Stan, C. H. Schunck, M. W. Zwierlein, K. Dieckmann, and W. Ketterle, *Phys. Rev. Lett.* **91**, 160401 (2003).
[6] N. Navon, S. Nascimbène, F. Chevy, and C. Salomon, *Science* **328**, 729 (2010).
[7] M. J. H. Ku, A. T. Sommer, L. W. Cheuk, and M. W. Zwierlein, *Science* **335**, 563 (2012).
[8] C. Cao, E. Elliott, J. Joseph, H. Wu, J. Petricka, T. Schäfer, and J. E. Thomas, *Science* **331**, 58 (2011).
[9] T. Rom, Th. Best, D. van Oosten, U. Schneider, S. Fölling, B. Paredes, and I. Bloch, *Nature* **444**, 733 (2006).

- [10] D. Greif, T. Uehlinger, G. Jotzu, L. Tarruell, and T. Esslinger, *Science* **340**, 1307 (2013).
- [11] R. A. Hart, P. M. Duarte, T.-L. Yang, X. Liu, T. Paiva, E. Khatami, R. T. Scalettar, N. Trivedi, D. A. Huse, and R. G. Hulet, *Nature* **519**, 211 (2015).
- [12] P. A. Murthy, N. Defenu, L. Bayha, M. Holtén, P. M. Preiss, T. Enss, S. Jochim, *Science* **365**, 268 (2019).
- [13] N. Luick, L. Sobirey, M. Bohlen, V. P. Singh, L. Mathey, T. Lompe, H. Moritz, *Science* **369**, 89 (2020).
- [14] M. Lu, N. Q. Burdick, and B. L. Lev, *Phys. Rev. Lett.* **108**, 215301 (2012).
- [15] K. Aikawa, A. Frisch, M. Mark, S. Baier, R. Grimm, and F. Ferlaino, *Phys. Rev. Lett.* **112**, 010404 (2014).
- [16] A. Frisch, M. Mark, K. Aikawa, F. Ferlaino, J. L. Bohn, C. Makrides, A. Petrov, and S. Kotochigova, *Nature* **507**, 475 (2014).
- [17] M. Schmitt, M. Wenzel, F. Böttcher, I. Ferrier-Barbut, and T. Pfau, *Nature* **539**, 259 (2016).
- [18] L. Chomaz, S. Baier, D. Petter, M. J. Mark, F. Wächtler, L. Santos, and F. Ferlaino, *Phys. Rev. X* **6**, 041039 (2016).
- [19] C. R. Cabrera, L. Tanzi, J. Sanz, B. Naylor, P. Thomas, P. Cheiney, and L. Tarruell, *Science* **359**, 301 (2018).
- [20] G. Semeghini, G. Ferioli, L. Masi, C. Mazzinghi, L. Wolswijk, F. Minardi, M. Modugno, G. Modugno, M. Inguscio, and M. Fattori, *Phys. Rev. Lett.* **120**, 235301 (2018).
- [21] C. D'Errico, A. Burchianti, M. Prevedelli, L. Salasnich, F. Ancilotto, M. Modugno, F. Minardi, and C. Fort, *Phys. Rev. Research* **1**, 033155 (2019).
- [22] D. Rakshit, T. Karpiuk, M. Brewczyk, and M. Gajda, *SciPost Phys.* **6**, 079 (2019).
- [23] D. Rakshit, T. Karpiuk, P. Zin, M. Brewczyk, M. Lewenstein, and M. Gajda, *New J. Phys.* **21**, 073027 (2019).
- [24] T. Karpiuk, M. Nikolajuk, M. Gajda, and M. Brewczyk, *Sci. Rep.* **11**, 2286 (2021).
- [25] M. Nikolajuk, T. Karpiuk, L. Ducci, and M. Brewczyk, *ApJ* **980**, 256 (2025).
- [26] G. R. Sivakoff, C. L. Sarazin, and A. Jordán, *Astrophys. J.* **624**, L17 (2005).
- [27] J. A. Irwin, W. P. Maksym, G. R. Sivakoff, A. J. Romanowsky, D. Lin, T. Speegle, I. Prado, D. Mildebrath, J. Strader, J. Liu, and J. M. Miller, *Nature* **538**, 356 (2016).
- [28] G. Spada, S. Pilati, and S. Giorgini, *Phys. Rev. Lett.* **131**, 173404 (2023).
- [29] G. Spada, S. Pilati, and S. Giorgini, *Phys. Rev. Lett.* **133**, 083401 (2024).
- [30] K. Gawryluk, T. Karpiuk, M. Gajda, K. Rzążewski, and M. Brewczyk, *Int. J. Comput. Math.* **95**, 2143 (2018).
- [31] T. Świsłocki, K. Gawryluk, M. Brewczyk, and T. Karpiuk, *Comput. Phys. Commun.* **318**, 109897 (2026).
- [32] B. J. DeSalvo, K. Patel, J. Johansen, and C. Chin, *Phys. Rev. Lett.* **119**, 233401 (2017).
- [33] B. J. DeSalvo, K. Patel, G. Cai, and C. Chin, *Nature* **568**, 61 (2019).
- [34] R. Pires, J. Ulmanis, S. Häfner, M. Repp, A. Arias, E. D. Kuhnle, and M. Weidemüller, *Phys. Rev. Lett.* **112**, 250404 (2014).
- [35] E. Lippi, M. Gerken, S. Häfner, M. Repp, R. Pires, M. Rautenberg, T. Krom, E. D. Kuhnle, B. Tran, J. Ulmanis, B. Zhu, L. Chomaz, and M. Weidemüller, *Few-Body Syst.* **66**, 1 (2025).
- [36] M. Brewczyk, M. Gajda, and K. Rzążewski, *J. Phys. B* **40**, R1 (2007).
- [37] <https://youtu.be/uoYmB3y7Hj4>.
- [38] <https://youtu.be/iBZU0RvBIkM>.
- [39] <https://youtu.be/K4a94Tav6jE>.
- [40] <https://youtu.be/ZcnYA1b2pWQ>.
- [41] E. Madelung, *Z. Phys.* **40**, 322 (1927).
- [42] H. Frölich, *Physica* **37**, 215 (1967).
- [43] C. Y. Wong and J. A. McDonald, *Phys. Rev. C* **16**, 1196 (1977).
- [44] N. H. March and B. M. Deb, *The single-particle density in physics and chemistry* (Academic Press, London, 1987).
- [45] P. T. Grochowski, T. Karpiuk, M. Brewczyk, and K. Rzążewski, *Phys. Rev. Lett.* **119**, 215303 (2017).
- [46] P. T. Grochowski, T. Karpiuk, M. Brewczyk, and K. Rzążewski, *Phys. Rev. Lett.* **125**, 103401 (2020).
- [47] T. Karpiuk, M. Gajda, and M. Brewczyk, *New J. Phys.* **22**, 103025 (2020).
- [48] J. Ryszkiewicz, M. Brewczyk, and T. Karpiuk, *Phys. Rev. A* **105**, 023315 (2022).
- [49] C. Pethick and H. Smith, *Bose-Einstein Condensation in Dilute Gases* (Cambridge University Press, Cambridge, 2002).
- [50] K. Huang, *Statistical Mechanics* (Wiley, 2014).